

# Mid-infrared Imaging of Nearby Radio-Loud AGN

**Eric S. Perlman<sup>1</sup>, Matthew Merlo<sup>1</sup>, Chris Packham<sup>2</sup>, Rachel Mason<sup>3</sup>, and Los Piratas.**

<sup>1</sup> Department of Physics & Space Sciences, Florida Institute of Technology, 150 W. University Blvd., Melbourne, FL 32901, USA

<sup>2</sup> Department of Physics & Astronomy, University of Texas at San Antonio, 1 UTSA Circle, San Antonio, TX 78249, USA

<sup>3</sup> Gemini Observatories, 670 N. A'ohoku Place, Hilo, HI 96720, USA

## Abstract

We present high spatial resolution MIR observations for several nearby radio loud active galactic nuclei (RLAGN), which were obtained using the Gemini North and South telescopes. Of the six observed objects, we detected five in the Si-2 (8.7 microns) and Si-6 (12.3 microns) filters, of which two objects show some evidence of low level extended emission surrounding the unresolved nucleus. In Pictor A, we also obtained an image in Qs (18.3 microns) that has a flux of only half that seen in the Spitzer image, suggesting structure on arcsecond scales. We also used the Si-6 (12.3 microns) flux measurement to investigate correlation between our MIR flux and xray luminosity and compare this to results for AGN in general. This work also forms a basis for future high resolution imaging and spectroscopy of these objects.

## 1 Introduction

Active galactic nuclei (AGN) include many different object classes with drastically different properties, from ultra-luminous quasars to Seyfert galaxies to galaxies with powerful radio jets. These diverse classes span as many as eight decades in luminosity, include objects with and without broad optical emission lines, and have varied SED shapes. One of the major developments in the study of AGN was the proposal of a unified theory, which allows these vastly different observed properties to be explained by one structure, instead of a different type of system for each type of object. The unified theory proposes a system with a super-massive black hole, accretion disk and fast-moving broad line clouds within the inner 0.1 pc, surrounded by an optically-thick torus of dust and gas with narrow line clouds present at larger radii (see e.g., [1, 24] for reviews). The torus absorbs the x-ray, UV, and optical

emission from the central engine and re-emits it in the infrared. This makes mid-infrared (MIR) observations particularly useful for studying the torus and its surroundings through both imaging and spectroscopy.

While significant strides have been made in the understanding of the MIR emission of the "radio quiet" (RQ) population of AGN, much less work has been done with "radio loud" (RL) AGN. About 10-20% of AGN have strong radio emission. These RLAGN have powerful radio jets, as opposed to the larger RQ population, which have very small, low-power jets or none at all. Jets emit via non-thermal processes, in particular via synchrotron radiation and (particularly at UV and higher frequencies) a variety of inverse-Compton mechanisms. This non-thermal emission dominates the properties of the source in the radio and mm, where the luminosity of RL AGN can be orders of magnitude higher than that of RQ AGN, but at near-infrared to X-ray wavelengths, RL and RQ AGN have remarkably similar broadband spectral properties (see e.g., [16]). This indicates that, in particular, the optical and near-infrared emission of RL and RQ AGN are similar in nature, emerging from similar processes and regions of the AGN. In the mid-to-far infrared, however, the thermal emission from the torus must compete with emission from the high energy tail of the synchrotron component. Simple power-law extrapolations of the radio and near-infrared spectra of RL AGN (e.g., [6]) indicate that the crossing point for the thermal and non-thermal emission components should be somewhere in the infrared. Thus in some objects it is possible that the majority of the MIR emission may not come from warm dust in the AGN central regions (e.g., M87, [18]), thus leaving open the question of the MIR continuum's nature.

With this context in mind, then, mid-infrared observations of RL AGN at high angular resolution are of considerable importance. Yet, to date, by far the majority of high angular resolution, MIR observations of AGN are of RQ objects, with only a small number of RL objects having been observed. Recent MIR observations have started to fill in our knowledge of RL AGN. MIR imaging of M87 shows a unresolved nucleus with a large radio jet with synchrotron emission from both the nucleus and extended jet [18, 23], while the MIR imaging of Cen A shows an unresolved synchrotron nucleus surround by MIR emission from both dust and star-formation surrounding the nucleus [19]. The MIR imaging of Cen A also was able to place an upper limit of 4pc on the torus, which is consistent with findings from VLT interferometry [13]. MIR imaging of Cyg A revealed a complex picture, with a bright central source and a biconical, dusty emission region [20]. These structures resembled those seen with HST optical and near-IR observations [7, 21]. These observations show the potential of high resolution MIR observations of RLAGN and highlights the need for these type of observations for a larger number of RLAGN. Also, these three objects also have high resolution MIR spectroscopy observations [17, 13, 5, 15].

Other imaging observations are now being made, filling in one side of the story. For example, a larger high resolution imaging survey of RL AGN was presented in [22]. Another 6, lower-luminosity objects were presented in [14] as part of their work on mid-IR imaging of LINERs. In this paper, we will present multiband MIR imaging for six nearby (i.e  $z < 0.1$ ), bright (i.e. N band flux  $> 50$  mJy in ISO and/or *Spitzer* observations) RL AGN. Along with the information gained from these observations, they will set the stage for future high resolution spectroscopy, allowing a complete picture of the objects to be obtained.

## 2 Results

MIR imaging observations were taken for six nearby RL-AGN using the 8.1m Gemini North and South telescopes and their respective mid-IR imaging cameras Michelle and T-ReCS. The objects were selected to have  $12\ \mu\text{m}$  flux  $> 50$  mJy in ISO and/or *Spitzer* observations. Table 1 lists critical information for these objects.

For our observations, three different filters were used: the Si-2 filter centered at  $8.7\ \mu\text{m}$  with a bandwidth of  $0.9\ \mu\text{m}$ , the Si-6 filter centered at  $12.3\ \mu\text{m}$  with a bandwidth of  $1.2\ \mu\text{m}$ , the Qa filter centered at  $18.3\ \mu\text{m}$  with a bandwidth of  $1.5\ \mu\text{m}$ . This allows us to observe both continuum and line emission, with a spatial resolution of  $\sim 0.3''$ , about  $10\times$  greater than that of *Spitzer* ( $\sim 3''$ ). Typical observing times were 10 minutes per band on-source, with the exception of Pictor A, where much deeper observations ( $\sim 1.5$  hours on source) were obtained at  $8.7$  and  $12.3\ \mu\text{m}$ . In [15] we also give the details of our observations and data reduction procedures. We note that the upper limit given for M84 is at the  $2\ \sigma$  level and agrees with the observations of [14].

Object Name	Redshift	F(8.7)	F(12.3) mJy	F(18.3)
3C84	0.0176	$372 \pm 4$	$621 \pm 6$	...
3C120	0.0330	$110 \pm 1$	$226 \pm 2$	...
M84	0.00354	$< 1.1$	$< 8.8$	...
Cen B	0.0129	$35.1 \pm 0.6$	$64 \pm 1$	...
Fornax A	0.00587	$8.1 \pm 0.5$	$5.5 \pm 0.2$	...
Pic A	0.0351	$31 \pm 6$	$54 \pm 1$	$55 \pm 5$

Table 1: Our sample of RL-AGN.

Figure 1 shows images for three objects: 3C 84, 3C 120 and Pictor A. The contour levels shown are based on the rms noise found in the images  $\sigma$ , showing 1,2,3,4,5, 10, 15, and 20  $\sigma$  above background. All of these images show a strong unresolved source, a common feature of all of our images. In a few cases we find evidence of extended emission. For example, the  $12.3\ \mu\text{m}$  image of 3C 84 shows circularly symmetric extended flux at radii  $> 0.4''$ . We show the radial profile of that object in Figure 2, compared to the profile for the PSF standard observed immediately before. This emission could be due to circumnuclear star formation, given the  $\text{H}\alpha$  filaments known in 3C 84's host galaxy and the presence of PAH lines in the *Spitzer* spectrum [10]. Deeper observations are required to untangle this subject.

## 3 Correlation between X-ray and MIR Luminosity and Discussion

The MIR ( $12\ \mu\text{m}$ ) and hard X-ray (2-10 keV) luminosities of AGN are well correlated, as first reported by [8] and [12] based on ISO data. This correlation was elaborated on using

ground-based data by [4], and refined by [11] and [3] who used data for objects with  $< 100pc$  resolution as well as absorption-corrected X-ray luminosity. This correlation is beginning to be explored for radio loud objects as well. [2] added the radio-loud AGN observed to date to that correlation. Here we add the radio-loud AGN of this work and also [14] and [22] to that plot, using the mid-IR luminosity within a 100 pc region where available, as in [11]. This plot is shown in Figure 3.

As can be seen, the RL AGN do not differ significantly from RQ AGN. The RL AGN show a highly significant correlation, with a Spearman rank order correlation coefficient,  $\rho=0.797$ , corresponding to a null hypothesis probability of  $p=6.28 \times 10^{-4}$ . There is no significant difference between the slopes of the two classes. While this is less secure than for all the AGN plotted ( $\rho = 0.926, p = 1.69 \times 10^{-38}$ ), this is purely a result of the smaller number of RL AGN observed. The fact that this correlation seems to hold for both RL AGN and RQ QGN indicates that the X-ray luminosity can be linked to that in the mid-IR in a similar way for all AGN, regardless of radio loudness. Our results also indicate that for most RL AGN, the mid-IR band is dominated by physical processes similar to those seen in RQ AGN, i.e., thermal emission from the torus and/or star formation, with a more minor contribution from non-thermal synchrotron emission – although exceptions such as M87 certainly exist. The only difference between classes appears to be for the LINERs, which do appear to skew the correlation somewhat. We are investigating this last observation further.

[4] and [11] interpreted the correlation as evidence for a compact, clumpy torus, as opposed to a much larger one that is smooth in morphology [9]. A larger but smooth torus would also have correlated MIR and X-ray luminosities, but with a larger mean value of  $L_{MIR}/L_X$  for Sy 1s than Sy 2s, which is not seen in RQ AGN (e.g., [11, 3, 4]). While the RL AGN are also consistent with no differences between the Sy 1 and Sy 2 correlation, this statement cannot be made securely as there are too many upper limits on the MIR luminosity (particularly in the work of [22]). The data thus lead us to infer that the tori of RL AGN are of roughly similar size and morphology as those of RQ AGN – namely, being sub-parsec in size. This is a significantly tighter constraint than we can gain using our imaging data alone, where due to the greater distances of the objects we can only constrain the size of the tori to  $\sim 10 - 50$  pc. We will explore this issue in a later paper.

## References

- [1] Antonucci, R. R. J., 1993, ARAA, 31, 473
- [2] Asmus, D., et al., 2011, A&A, 2011, A&A 2011, 536, 36
- [3] Gandhi, P., et al., 2009, A& A, 502, 457
- [4] Horst, H., et al., 2008, A& A, 479, 389
- [5] Imanishi, M., & Ueno, S., 2000, ApJ, 545, 626
- [6] Impey, C. D., Neugebauer, G., 1988, AJ, 95 ,307
- [7] Jackson, N., Tadhunter, C., & Sparks, W. B., 1998, MNRAS, 301, 131

- [8] Krabbe, A., Böker, T., & Maiolino, R., 2001, *ApJ*, 557, 626
- [9] Krolik, J. H., & Begelman, M. C., 1988, *ApJ*, 329, 702
- [10] Leipski, C., et al., 2009, *ApJ*, 701, 891
- [11] Levenson, N. A., et al., 2009, *ApJ*, 678, 729
- [12] Lutz, D., et al., 2004, *A& A*, 418, 465
- [13] Meisenheimer, K., et al., 2007, *A& A*, 471, 453
- [14] Mason, R. E., et al., 2012, *AJ*, 144, 11
- [15] Merlo, M., et al., 2013, in prep.
- [16] Perlman, E. S., 2012, in *Planets, Stars & Stellar Systems*, vol. 6
- [17] Perlman, E. S., et al., 2007, *ApJ*, 663, 808
- [18] Perlman, E. S., et al., 2001, *ApJ*, 561, L51
- [19] Radomski, J. T., et al., 2008, *ApJ*, 681, 141
- [20] Radomski, J. T., et al., 2002, *ApJ*, 566, 675
- [21] Tadhunter, C. N., et al., 1999, *ApJL*, 512, L91
- [22] van der Wolk, G., et al., 2010, *A&A*, 511, 64
- [23] Whysong, D., & Antonucci, R., 2004, *ApJ*, 602, 116
- [24] Urry, C. M., & Padovani, P., 1995, *PASP*, 107, 803

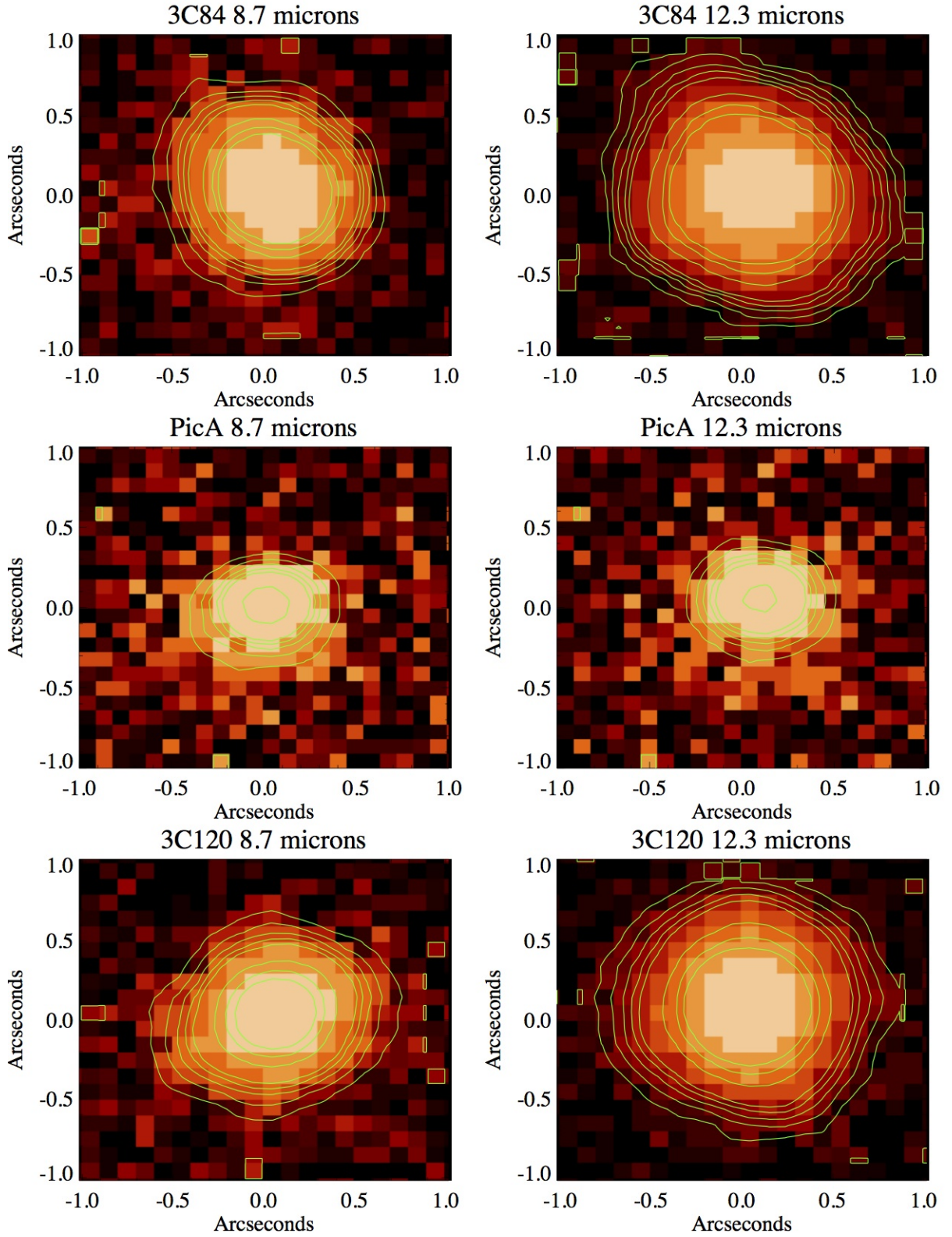


Figure 1: Mid-IR images of 3C 84, 3C 120 and Pic A at  $8.7 \mu\text{m}$  and  $12.3 \mu\text{m}$ . Contours are plotted at 1, 2, 3, 4, 5, 10, 15 and 20  $\sigma$  above the background.

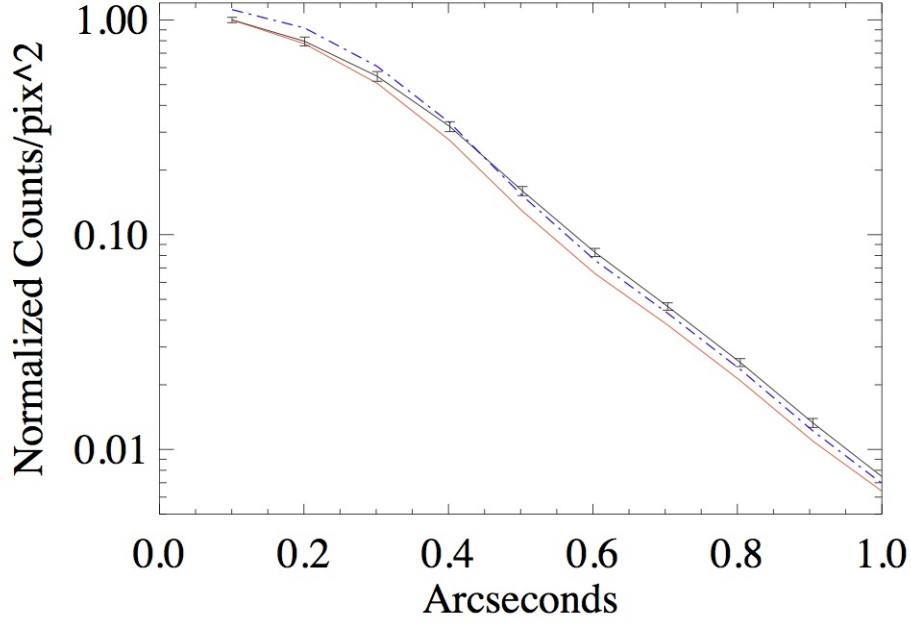


Figure 2: The radial profile for 3C 84 at  $12.3 \mu\text{m}$  (points, with  $1\sigma$  error ranges shown, and black curve). Plotted for comparison are the PSF as derived from a flux calibration star observed the same night (red curve), as well as a curve at  $3\sigma$  above the PSF (dash-dot curve).

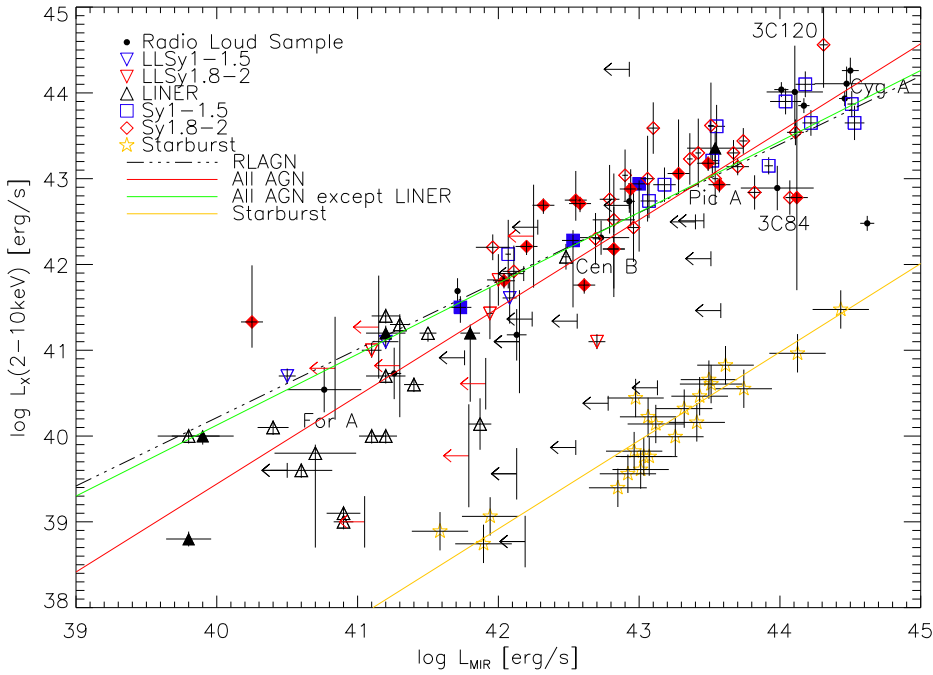


Figure 3: The mid-IR vs. X-ray luminosity correlation for radio-loud as well as radio-quiet AGN. See Section 3 for discussion.